Ferrimagnetic Resonance in Rare-Earth Doped Yttrium Iron Garnet.
II. Terbium Substitution

J. F. DILLON, JR., AND L. R. WALKER

Bell Telephone Laboratories, Murray Hill, New Jersey

The replacement of a small fraction of the yttrium ions in yttrium iron garnet by rare-earth ions produces large effects on the field for ferrimagnetic resonance at low temperatures. Detailed studies have been made on the effect of terbium substitution using concentrations from 0.01 to 0.19 at. %. The variation of the field for resonance as a function of applied field direction, of temperature, and of frequency are examined. The field for resonance has been calculated by evaluating the rf susceptibility and dc magnetization of the terbium ions from their energy levels and wave functions in assumed crystal and exchange fields. The calculated fields show good qualitative agreement with the facts; quantitative agreement would require more flexibility in the choice of a crystal field.

THE substitution for yttrium of small amounts of various rare earths produces very marked effects upon the ferrimagnetic resonance of yttrium iron garnet.[1,2] In particular, earlier work showed that the field for resonance at low temperatures ($<10°K$) and with impurity concentrations of a fraction of a percent, may change by several kilo-oersteds when the direction of the applied magnetic steady field is altered by a few degrees. It was also found that even when the resonance field was varying slowly with orientation, its value was many hundreds of oersteds below that for an undoped sample. Terbium substitution produced these effects in the most striking fashion, and for this reason, an extended experimental study has been made of this element. At the same time an attempt was made to compute the field for resonance on the basis of a simple model.

A qualitative explanation of the excursions of the field for resonance with field direction has been given previously.[3] We shall first review the somewhat more detailed model which we have used. The doped crystal may be treated as a two-sublattice system; the strongly-coupled iron sublattices form one of these and the terbium ions, which in the concentrations used ($<0.2\%$) may be considered to move independently of each other, form the second. The majority sublattice magnetization $\mathbf{M}$ may be supposed to obey the small signal version of the equation

$$d\mathbf{M}/dt = \gamma(\mathbf{M} \times \mathbf{H}_{eff}),$$

where γ is the appropriate gyromagnetic ratio and $\mathbf{H}_{eff}$ is the total effective magnetic field. The latter will include in addition to the applied magnetic field and the iron anisotropy field, the exchange field of the terbium sublattice. There will be a dc contribution to this field from the component of the dc magnetization of the terbium along the applied field and an rf contribution

from the induced rf moment of the terbium in a plane normal to this direction. The dc and rf moments of the terbium are in turn produced by the combined action of the crystalline field and the dc and rf exchange fields of the iron lattice. Because the dc exchange field and the crystalline field are comparable in magnitude, it is necessary to calculate initially the exact energy levels and wave functions of the terbium ions. From these we may calculate first the dc moment of the terbium. Secondly, having written down an expression for the rf moment induced as a result of the action of rf exchange field, we may actually evaluate this. Enough equations are now available to calculate the field for resonance of the combined system.

Large excursions of the field for resonance are now to be associated with large changes in the rf susceptibility of the terbium as a function of the applied field's direction. At low temperatures, when only the lowest terbium energy level is populated, the susceptibility will vary rapidly if the ground- and first-excited levels approach closely at some angle and at the same time the matrix element for transitions between these levels has an appreciable value. The sharpness of the angular variations may be expected to decrease as the temperature rises and more levels are populated. Since the denominators in the expression for the susceptibility contain the driving frequency, one may expect to see frequency dependence of the angular behavior other than that which arises from the associated change of applied field with frequency. At angles for which the lowest energy levels do not approach closely, one may still expect to see a change in the field for resonance caused by the terbium impurity. For, though in the absence of a strong crystal field the dc and rf exchange fields acting on the majority lattice are so related as to leave no exchange term in the field for resonance (this is the familiar case), this cancellation does not take place in general.

An analysis of the above model could be carried through completely if the crystal potential and exchange field at the terbium sites were known. Unfortunately, we have no information about the former and the latter is known only through an analysis which

[1] J. F. Dillon, Jr., and J. W. Nielsen, Phys. Rev. Letters **3**, 30 (1959).

[2] J. F. Dillon, Jr., and J. W. Nielsen, Phys. Rev. **120**, 105 (1960). Hereafter referred to as I.

[3] C. Kittel. Phys. Rev. Letters **3**, 169 (1959); Phys. Rev. **117**, 681 (1960). The model considered here is somewhat more detailed than Kittel's and leads to some additional consequences.
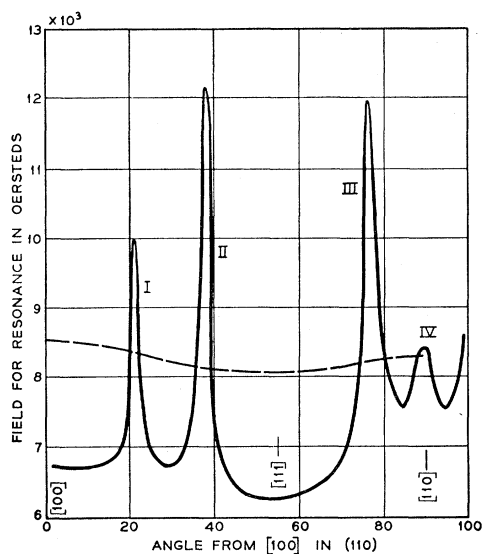
FIG. 1. H_{res} in (110) at 1.5°K in YIG(0.2% Tb). The frequency was 22 989 Mc/sec. The peaks as seen in this plane are designated by Roman numerals. The dashed curve is H_{res} for the purest YIG with which we have worked.

ignores the effects of crystal fields upon the magnetization curve of terbium iron garnet.[4] We have therefore used a Hamiltonian with a few adjustable parameters based primarily upon the point-charge model. It turns out that a fairly satisfactory fit to the observed data may be obtained. The agreement is good qualitatively, but never really excellent quantitatively. There appears to be a range for each of the adjustable parameters which leads to about the same degree of agreement. In view of the tentative nature of the fitting it has not seemed worthwhile to do more than discuss the questions of temperature and frequency dependence in a qualitative way.

EXPERIMENTS

Samples

The crystals were grown under the direction of Nielsen.[5] The crystal growth was done in an oxygen

TABLE I. Intended and measured terbium concentrations in a number of samples.

Intended dilution (atomic %)	Analysis (atomic %)	R = Measured/ intended
1.13	1.7	1.5
0.25	0.30	1.2
0.19	0.28	1.5
0.05	0.058	1.2
0.019	0.025	1.3
0.010	0.015	1.5

[4] R. Pauthenet, thesis, Universite de Grenoble, 1958 (Masson, Paris, France, 1958).
[5] J. W. Nielsen, J. Appl. Phys. 31, 51S (1960). We wish to thank Dr. Nielsen for providing these samples.

atmosphere from lead oxide-lead fluoride flux. Though earlier analyses for terbium were not meaningful in the range of interest, Shirley Vincent of these Laboratories has recently performed x-ray fluorescence analyses of crystals taken from the same growth runs as our samples. She believes these to be good to within 5% of the amount of Tb present. Table I gives these results along with the intended dilution. It will be seen that the ratio R of intended/measured terbium concentration varies in the range from about 1.2–1.5. Reference to a similar list of data for all of the rare earths given in Table I of I, shows that most, but not all, of the rare earths from samarium to ytterbium gave a value of this ratio in about the same range. From the near consistency of these analyses it looks as if more terbium appears in the crystal than in the starting mixture. However, the spread in R from 1.2 to 1.5 in crystals which were grown at about the same rate should be a basis for caution. Having made these remarks, we will continue to designate the samples as YIG (x% Tb) where the x% indicates the percentage of yttrium atoms in the starting mixture which have been replaced by terbium atoms.

It should be noted in passing that our H_{res} data provide an excellent indication of relative terbium concentrations down to a few parts per million.

The sample preparation and orientation procedures were described in I.

Apparatus

A great part of this work was performed at 20 and 24 kMc/sec using the apparatus described in I. Though we have recorded H_{res} vs angle curves automatically on an experimental basis, the very steep excursions of the field for resonance as well as the accompanying changes in linewidth, have made a point-by-point measurement of H_{res} at many angular settings more feasible.

The measurements at higher frequencies were made using a spectrometer recently described by Mock.[6] In these cases the field measurements were made with a rotating-coil gaussmeter. When possible, reference points were measured by counting the proton NMR frequency. The same spheres were used at the higher frequencies, as at 20 kMc/sec, and were thus generally larger than they should have been. Other modes than (110), the uniform precession, were frequently observed as will be seen later in Figs. 7 and 8. These high-frequency experiments were performed in open waveguides rather than in cavities, so the rf-field configuration could not be defined. Because of this, the size of the spheres, and the dielectric inhomogeneity introduced by the mounting rod, it was not possible to identify the uniform precession. Our procedure was to track in angle the field for resonance for several prominent modes. Of the several which could be followed through the necessary arc, it was invariably found that all

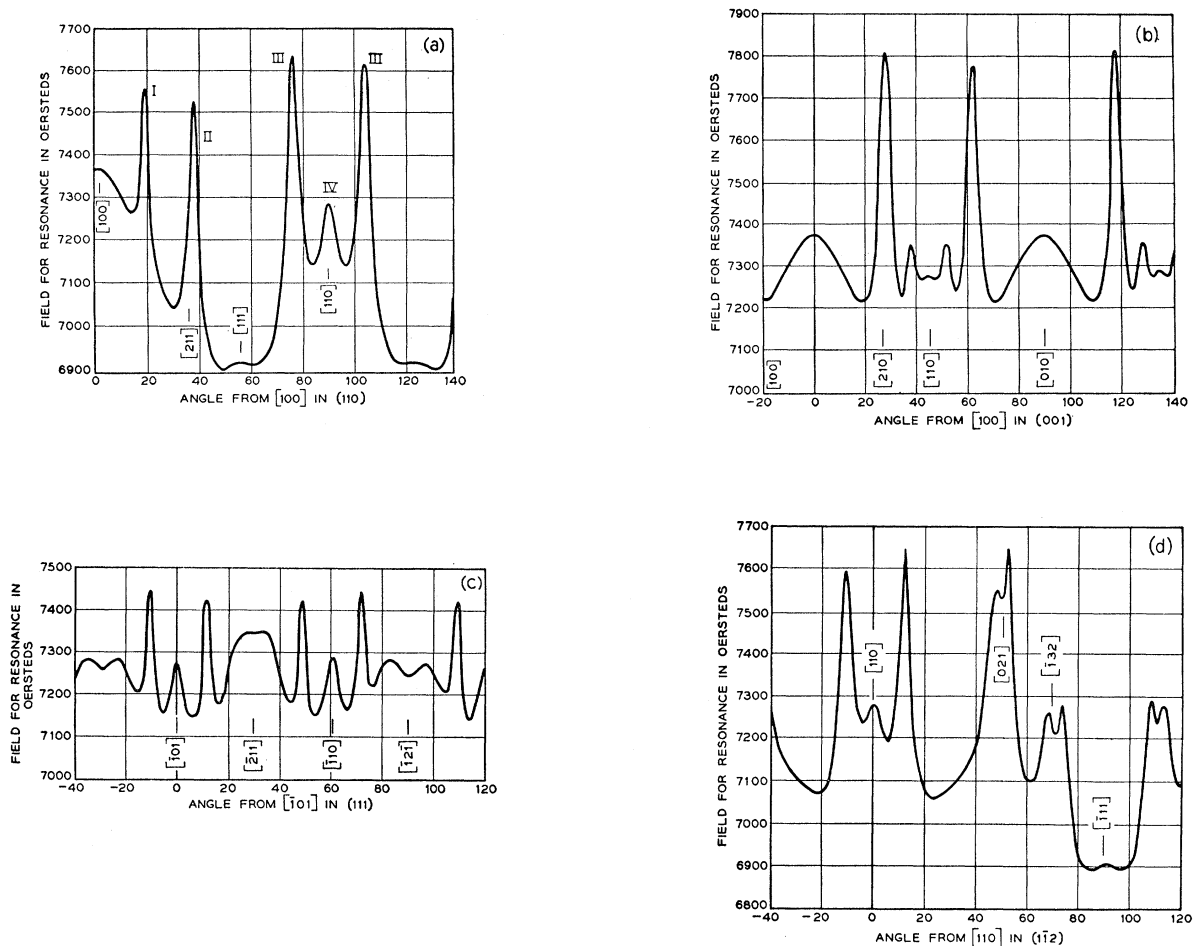[6] J. Mock, Rev. Sci. Instr. 31, 551 (1960).

FIG. 2. Four sections of the H_{res} surface of YIG (0.02% Tb) as measured at 1.5°K. Some of the important crystallographic directions are indicated for each of the planes. (a) The (110) section, at 20 228 Mc/sec; (b) the (001) section, at 20 240 Mc/sec; (c) the (111) section, at 20 221 Mc/sec; and (d) (112) section at 20 235 Mc/sec.

moved up and down in field together. That is, the various modes observed did not show different anisotropies.

Field for Resonance Surface

In a sample of YIG (0.2% Tb), H_{res} in (110) was observed as in Fig. 1. In this case the temperature was 1.5°K. The frequency was 23.0 kMc/sec. The corresponding data for pure YIG are given as the dashed curve. The salient feature of this plot is the set of high sharp peaks. Here and elsewhere in the paper we will designate these by I, II, III, and IV in order starting from [100]. By plotting these peaks on an expanded horizontal scale, we can measure an angular half-width for each. For I this is about 1.9°, for II it is 2.4° and for III it is 3.9°. Because of the slight overlap of III and IV, no attempt has been made to assign such a number to IV. On one side of II, the field for resonance falls by 4000 oe in one degree. We were not able to observe any hysteresis in this curve. Increasing the angle yields the same plot as decreasing the angle. Note that the field for resonance away from the peaks is depressed considerably below that for pure YIG.

Though measurements at several other temperatures were made for this sample, further experiments were concentrated on samples containing a lower percentage of terbium. These gave smaller excursions of the field for resonance, but had associated with them much narrower resonance lines. Thus, it was possible to follow the field for resonance contribution of the Tb ion with essentially the same accuracy, but without the vast changes in field which considerably slowed down the observations on more concentrated samples.

Figure 2 shows the field for resonance as measured in different crystallographic planes. These data were taken on spheres of YIG (0.02% Tb) at 1.5°K at a frequency of 20 kMc/sec. We shall refer back to the first curve, that of H_{res} in (110), in considering the variation with concentration, temperature, and frequency. At this level of concentration we can see the shape of the underlying H_{res} curve for undoped YIG, but super-
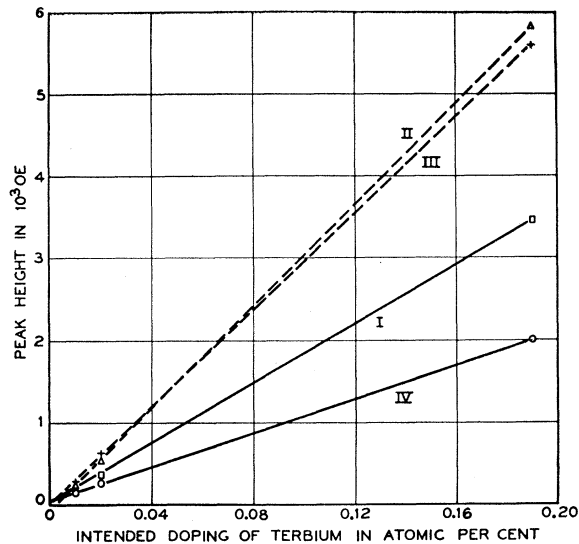
FIG. 3. A plot of peak height data against concentration of Tb in YIG. The numbers refers to the peaks shown in Figs. 1 and 2(a). Though there are only points at both ends of the line, it does seem that the peak height varies with concentration in this range.

imposed on it are the four peaks, I, II, III, and IV. The slight bump in the curve at [111] is probably associated with a tiny dysprosium impurity introduced in the yttrium used in this particular batch of crystals.

The highest values of the field for resonance are observed in the (100) plane. The slight variation from perfect symmetry observable here and in the (111) section reflect slight misorientations. In the (111) case, the field for resonance should be the same at $-30°$, $+30°$, and $+90°$, but the measured fields varied by about 100 oe. That this only represents a small misorientation can be understood when it is realized that this point is the [11$\bar{2}$] direction, the intersection of (111) and (1$\bar{1}$0). In the section of the (110) plane, Fig. 2(a), it is at 35.5°, the steep side of peak II.

It might be supposed that given the three principal sections of the surface H_{res} (hkl), it would be a straightforward exercise to construct a model of the entire surface. This is not the case. If a model is constructed in which these curves, plotted in polar coordinates, are
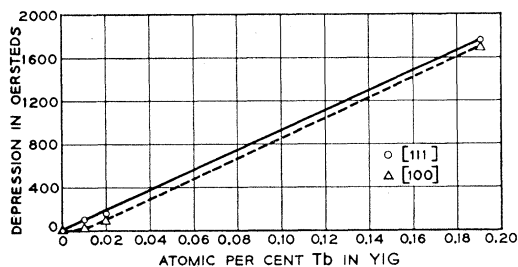

FIG. 4. In rare-earth-doped YIG, the field for resonance away from the peaks is depressed below that of pure YIG. This plot shows the magnitude of this depression for several concentrations of Tb in YIG. Cases of the field along [100] and [111] are plotted.

properly arranged in one octant, it is by no means obvious how they are to be joined. Thus, we were led to take data in the (112) plane and these are given in Fig. 2(d).

Concentration

We have observed these effects on the field for resonance surface in YIG crystals containing various levels of terbium doping. The height of the anomalous peaks in the anisotropy appears to vary linearly with concentration. Figure 3 shows the peak heights for three concentrations. Peak heights in this case were taken to be the field interval between the highest field for resonance of a particular anomaly and the corresponding field for pure YIG, the latter having been moved so as to correspond with the doped curve at [100].

Note in Fig. 1(a) that the field at which resonance occurs in these doped samples is significantly lower than in pure YIG. In Fig. 4 the values of this depression of the field for resonance are plotted for three samples of different concentrations. The cases of the field along
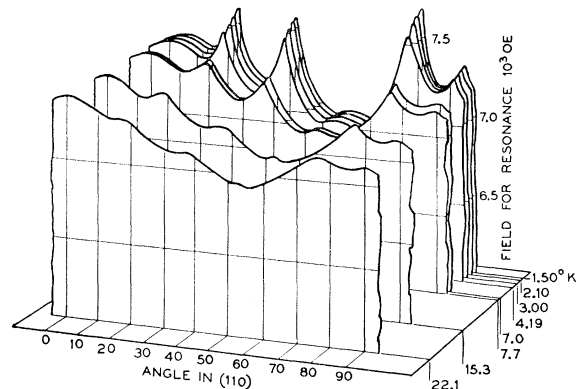

FIG. 5. The variation of the H_{res} [in (110)] curve with temperature for YIG(0.019 atomic % Tb). The data were taken at several frequencies near 20 200 Mc/sec, but the curves have been adjusted vertically slightly so that H_{100} appears at the same level in each plot.

[100] and [111] were measured. The [111] case seems to be perfectly linear, but the [100] curve starts off with a lower slope. The two lines have the same slope at high concentrations. This difference between the two depressions is curious, but well outside the experimental error in the measurement of field. Conceivably it might be a spurious effect associated with some other rare earth impurity in one or more of the samples.

Temperature

In Fig. 5 can be seen the way in which the field for resonance curve in (110) behaves as the temperature is raised. The anomalous peaks decrease in height and increase in width as the temperature increases. The line width of the resonance in these crystals increased up to about 90°K. The growing line breadth as well as

the reduced prominence of the structure make it difficult to resolve structure in an H_{res} curve much above about 50°K. A similar, though less complete set of measurements, were made at 51.6 kMc/sec. These curves are given in Fig. 6. Perhaps the most interesting feature here is the increased height of the peaks here as compared with the curves of Fig. 5. This we discuss below.

Frequency—Peak Height

The (110) section of the H_{res} surface at 1.5°K was determined for a sample of YIG (0.02% Tb) at frequencies from 9 to 73 kMc/sec. The high-frequency limit was set by the magnetic fields available. A variation was found both in the height of the anomalous peaks and in their angular position. In Fig. 7 the height of the anomalies is plotted against frequency directly. The height chosen here is the field interval between H_{res} in [111] and that at the top of the anomaly in question. Note the contrast already mentioned above. There is no change in IV, III goes approximately linearly, and II seems to be going somewhat faster than
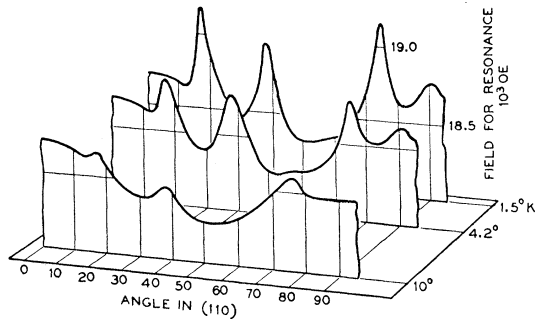
FIG. 6. Variation of H_{res} [in (110)] curve with temperature for YIG(0.019 atomic % Tb). These curves were taken 51 602 Mc/sec.

linearly at the higher frequencies. The height of the peak I near 18° increases very rapidly above about 50 kMc/sec. Just above 63 kMc/sec the linewidth becomes so broad that we are unable to locate it. The peak heights at 9.0 kMc/sec show an upward drift at the low-frequency end of the curves. Possibly this is associated with the failure of the low field to saturate the magnetization near the anomalies. An indication that this is occurring can be seen in the plot of peak position against angle in Fig. 10.

In the high-frequency spectrometer the sample is located in open waveguide on the end of a short piece of sapphire mounting rod. In this case we recorded the output of a detecting crystal as the field was varied. Thus, the output signal represents a combination of the real and imaginary parts of the permeability distorted by the characteristics of the detecting crystal and its associated circuitry. Figure 8 shows a sequence of output traces as the angle between the steady field and the [100] axis of the crystal is varied degree by degree
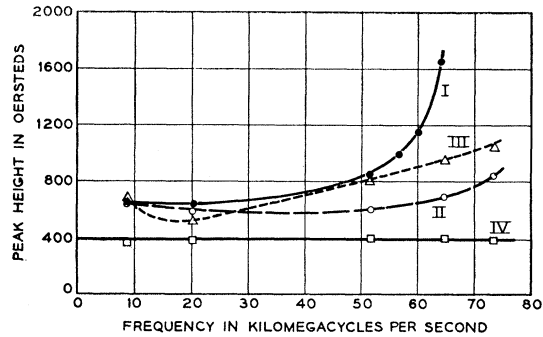
FIG. 7. The frequency variation of the height of the four peaks observed in the (110) section of H_{res} in YIG(0.02% Tb) at 1.5°K. The height plotted is that above H_{res} in [111].

near I. In this case, we seem to see only the absorption. There are a number of magnetostatic modes, and the line broadens considerably on passing over the peak at about 18°.

Figure 9 on the other hand, was taken at a somewhat higher frequency, 69.2 kMc/sec. At this frequency we see a mixture of dispersion and absorption, and do in fact, have a good deal more sensitivity than in Fig. 8. However, at the top of the peak, we see no signal. If the line is there, it is so broad that we could not assign a field to its position in a meaningful way.

As was noted in the introduction we interpret this blowup of one of the anomalous peaks as indicating that $h\nu$, the energy of the microwave quanta, approximates the energy gap between the two lowest levels of the terbium ground state. The losses associated with the excitation across this gap appear to be very large.

Frequency—Peak Position

In the (110) plane we find that the position at which the anomalous peaks occur shifts slightly with fre-

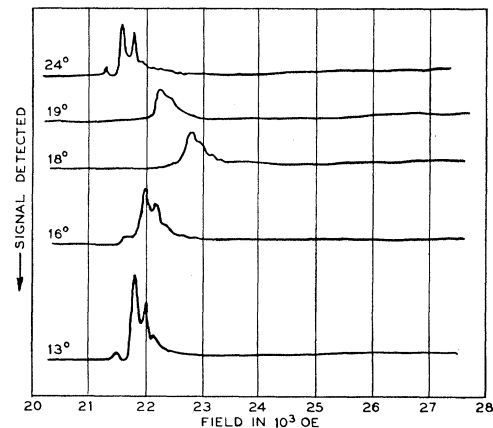FIG. 8. Variation of detected signal with applied magnetic field for the field along various direction in (110). The crystal was YIG(0.019 atomic % Tb). The temperature was 1.5°, and the frequency was 58 900 Mc/sec. Note that on passing through the peak at about 18° from [110] the line width increases considerably, but that it is still possible to follow the position of the line.
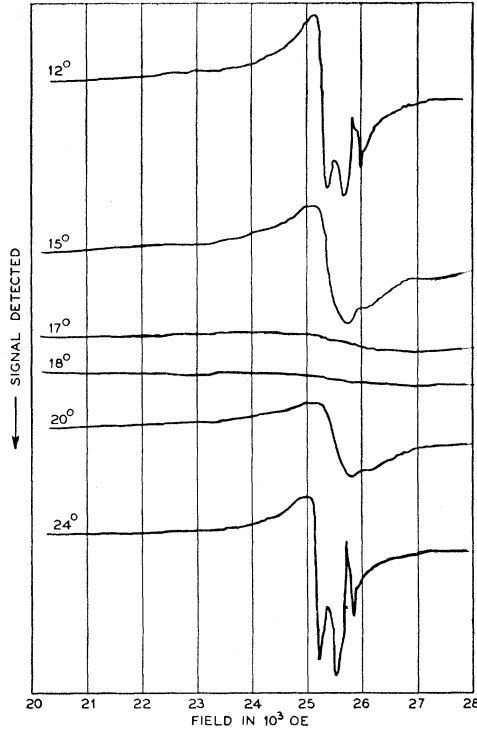
FIG. 9. Variation of detected signal with applied magnetic field for the field along various directions in the (110) plane. The crystal was of YIG (0.019 atomic % Tb). The numbers associated with each curve represent the angle from the [100] axis. These curves were taken at 69 200 Mc/sec. The temperature was 1.5°K.

quency, that is to say, with applied field. Peak IV which occurs along the [110] axis a symmetry direction does not shift. The angular locations are shown in Fig. 10. These measurements have been taken from a number of samples at various concentrations.

Above the lowest field set the points define straight lines rather well. Presumably, the bending at low fields can be ascribed to the failure to completely saturate the samples. The slopes of the straight lines on Fig. 10 are: I, $-1.1°/10^4$ oe; II, $1.35°/10^4$ oe; III, $-2.5°/10^4$ oe. That these peaks should shift with field is not at all unexpected, once it is realized that the phenomenon here arises from the splitting of the rare earth ground state by both electric and exchange fields. The shift to a higher frequency corresponds to the introduction of an increment of magnetic field, thus we are changing the relative contributions of the electric and magnetic fields.

ANALYSIS

The Hamiltonian

It was indicated earlier that in order to calculate the field for resonance one needs to know the dc magnetic moment and rf susceptibility of the terbium ions. To calculate these one must find the energy levels and wave functions of the terbium ion in the combined crystalline

and exchange fields. Unfortunately, the crystal field at the dodecahedral sites of YIG is not known independently. It is necessary, then, to attempt to find a plausible crystal field which will account for the facts. A starting estimate may be taken to be the potential of eight point charges at the oxygen sites surrounding each terbium ion.

There are six types of dodecahedral sites in YIG, each having the same orthorhombic symmetry when referred to a system of local axes, which differ, however in the spatial orientation of these axes (see Fig. 11). For any one of these sites the potential effective upon an f electron, referred to the local symmetry axes, will have the form

$$V = \lambda_0 Y_2^0 + \lambda_2 [Y_2^2 + Y_2^{-2}] + \mu_0 Y_4^0 + \mu_2 [Y_4^2 + Y_4^{-2}]$$
$$+ \mu_4 [Y_4^4 + Y_4^{-4}] + \nu_0 Y_6^0 + \nu_2 [Y_6^2 + Y_6^{-2}]$$
$$+ \nu_4 [Y_6^4 + Y_6^{-4}] + \nu_6 [Y_6^6 + Y_6^{-6}], \quad (1)$$

where the Y_n^m are spherical harmonics. In general, this expression contains nine constants. It is not feasible to attempt to vary every one of these in an attempt to fit the data. It has therefore been assumed that the point-charge model correctly gives the relative sizes of the constants within each order; in other words the ratios $\lambda_0 : \lambda_2$, $\mu_0 : \mu_2 : \mu_4$ and $\nu_0 : \nu_2 : \nu_4 : \nu_6$ are taken to be those of the point charge calculation. A justification for this particular way of simplifying the problem will be given when we go over to the spin Hamiltonian.

Since the ground state multiplet $(J=6)$ of the free terbium ion is separated by about 2000 cm^{-1} from the next multiplet, the crystalline spin Hamiltonian may set up for the $J=6$ manifold alone. Corresponding to Eq. (1) this will have the form

$$\mathcal{H}_{\mathrm{cryst}} = c_2 [\lambda_0 T_2^0 + \lambda_2 T_2^2] + c_4 [\mu_0 T_4^0 + \mu_2 T_4^2 + \mu_4 T_4^4]$$
$$+ c_6 [\nu_0 T_6^0 + \nu_2 T_6^2 + \nu_4 T_6^4 + \nu_6 T_6^6], \quad (2)$$

where the T's are the operator equivalents of the (real combinations of) spherical harmonics and c_{2r} is a constant, characteristic of the ground configuration, proportional to $\langle r^{2n} \rangle$, the $2n$th moment of the radial electron coordinate r for a terbium $4f$ wave function. Self-consistent field calculations have not been carried
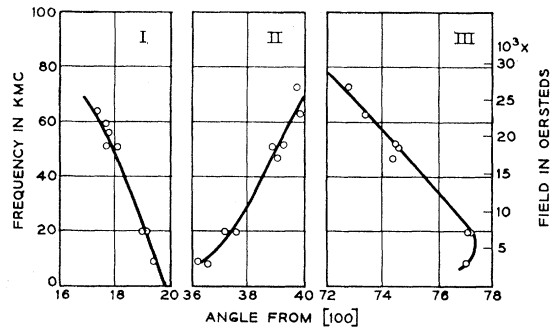

FIG. 10. The frequency (field) variation of the position of three of the peaks in H_{res} in the (110) plane of YIG(Tb) at 1.5°K.
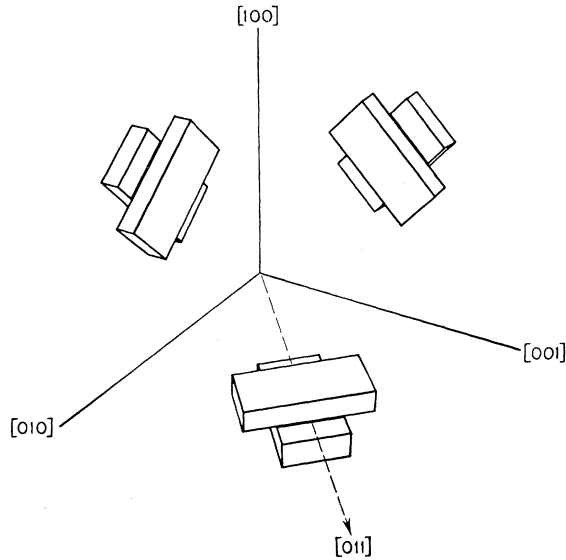
[100]

[010]

[001]

[011]

Fig. 11. The relative orientation of the six inequivalent types of dodecahedral site in YIG. Each parallelepiped represents the local orthorhombic symmetry of the sites. The indices refer to the crystallographic axes of the YIG crystal.

out for terbium ($Z=65$) and the $4f$ wave function to be used in calculating the moments has to be scaled from those of Au($Z=79$) or Tl($Z=81$). The screening parameter is of order 40 and the scaled wave functions are thus quite sensitive to the value chosen. The resultant uncertainty in the values of the c's supplies the reason for leaving them as three adjustable parameters. The values calculated from the scaled wave functions and the λ's, μ's and ν's calculated from the point charge model give an initial estimate of all the parameters in the crystal field Hamiltonian. For further details of the crystal spin Hamiltonian see the Appendix.

The exchange Hamiltonian will be of the form

$$\mathfrak{IC}_{ex}=\kappa(\mathbf{M}_0\cdot\boldsymbol{\sigma}_{Tb}),\tag{3}$$

where $\boldsymbol{\sigma}_{Tb}$ is the magnetic moment of a terbium ion ($|\sigma_{Tb}|=9$ Bohr magnetons), $\mathbf{M}_0$ is the saturation magnetization of the iron lattice and κ an appropriate molecular field constant. We identify the direction of $\mathbf{M}_0$ with the direction of the applied field. Here two effects are ignored. It will turn out that the direction of magnetization of the terbium ions does not coincide with that of the applied field and this will cause some local distortion in the alignment of the iron ions. Since the iron-iron exchange is very large this effect may be small. We are also ignoring the fact that the dc anisotropy which the terbium ions produce will give an equilibrium direction for the iron lattices which will not coincide with that of the applied field. Clearly inclusion of this effect would lead to a self-consistency problem of considerable complexity. It is to be expected that the calculated field for resonance curve will be somewhat distorted on the sides of the peaks by this misalignment

but the height of the peaks should not be greatly affected.

For an exploration of the two-lowest-energy levels as a function of angle with the object of finding a Hamiltonian which gives near crossings of these levels at the observed angles, it is sufficient to work with a dimensionless Hamiltonian. The exchange Hamiltonian for the ith site is therefore written as

$$\mathfrak{IC}_{ex}=\lambda(\mathbf{n}_i\cdot\mathbf{J}),\tag{4}$$

where $\mathbf{n}_i$ is a unit vector in the direction of the applied field and $\mathbf{J}$ is the total angular momentum operator in the $J=6$ manifold, λ is a dimensionless constant, $0<\lambda<1$. It is obviously convenient to work at each site in the axes which simplify the crystal field; the $\mathbf{n}_i$ then differ from site to site.

The working form of the Hamiltonian is taken to be, for the ith site,

$$\mathfrak{IC}=\lambda(\mathbf{n}_i\cdot\mathbf{J})+(1-\lambda)c_4'[(c_2/c_4)\mathfrak{IC}_2+\mathfrak{IC}_4+(c_6/c_4)\mathfrak{IC}_6],$$

where λ, c_2/c_4 and c_6/c_4 are the adjustable parameters, c_4' is a fixed number arranged to make the overall splitting in the pure exchange and pure crystalline cases roughly the same.[7] $\mathfrak{IC}_2$, $\mathfrak{IC}_4$, and $\mathfrak{IC}_6$ are the bracketed terms of (2). The choice of the energy scale will be discussed in the section on the field for resonance. When values of c_2/c_4 and c_6/c_4 are quoted later they will be expressed as multiples of the values of c_2/c_4 and c_6/c_4, respectively, estimated from the known thallium $4f$ functions (see Appendix).

Energy Levels

The calculation of the energy levels as a function of angle is free from some of the problems which arise in calculating the field for resonance and may be discussed separately.

We first found the eigenvalues of the dimensionless Hamiltonian as a function of angle in the (110) plane for various values of $\lambda,c_2/c_4,c_6/c_4$. It was possible to obtain a fairly good fit for the positions of the near-crossings (none in error by more than 5°) for values of λ between 0.8 and 0.3. For each value of λ in this range there is an associated range of values of c_2/c_4 and c_6/c_4 given by the approximate relation

$$\lambda=0.67(c_2/c_4)+0.22\pm0.10.$$

Values of λ outside this range might be used but it will be seen later that the fit of the field for resonance then becomes substantially poorer. The angular positions are not very sensitive to the value of c_6/c_4. Generally, $c_2c_6/(c_4)^2\sim1$ gives a good fit, but c_6/c_4 can be varied by about 50% from this value. If other factors are ignored, an error in the scaling of the wave functions alone would leave $c_2c_6/(c_4)^2=1$. Figure 12 shows the energy

[7] R. L. White and J. P. Andelin, Jr., Phys. Rev. 115, 1435 (1959).
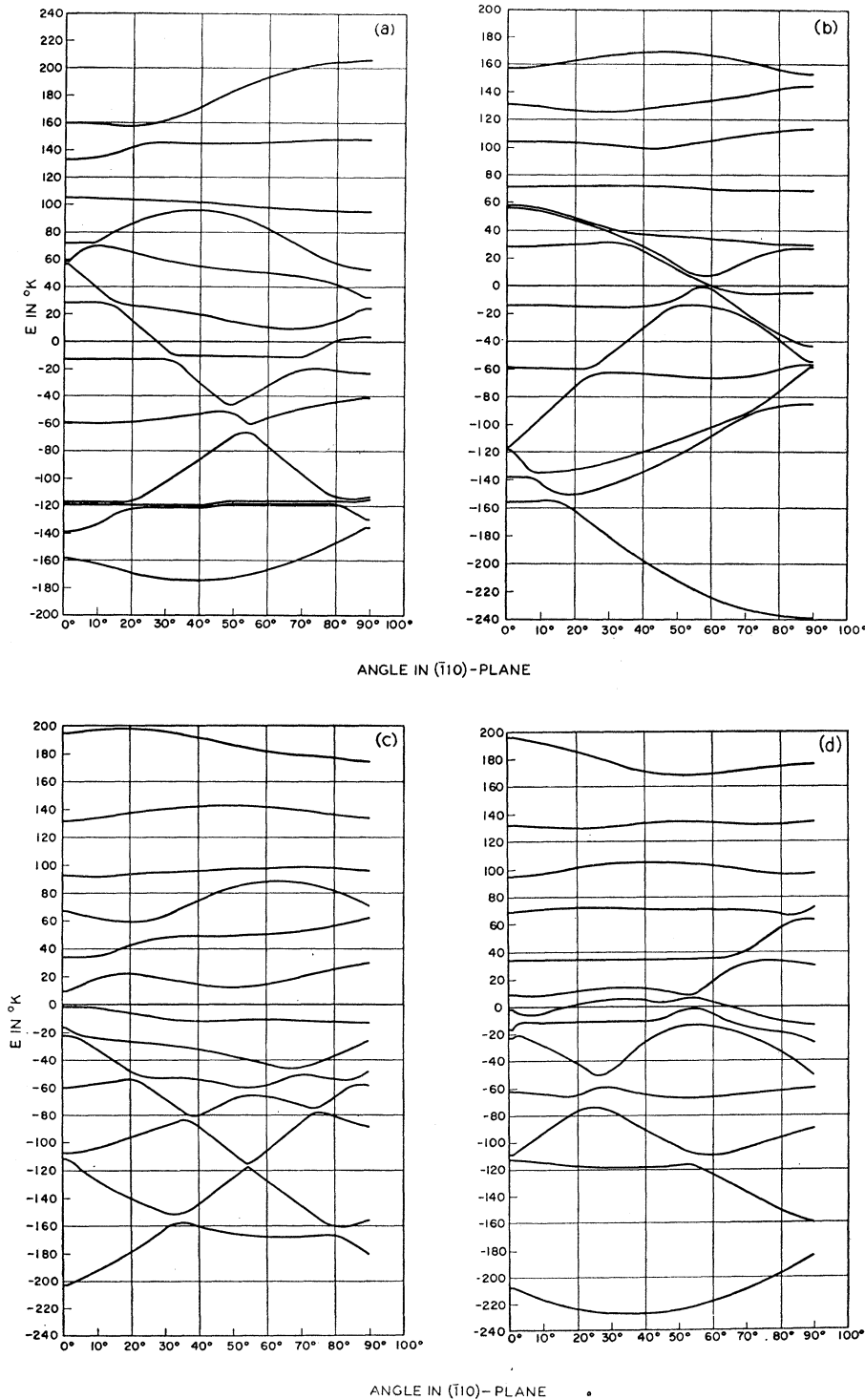
ANGLE IN (Ī10)-PLANE

FIG. 12. Energy levels for the four inequivalent sites as a function of the angle in the (110) plane between the [100] axis and the direction of magnetization for the case $\lambda=0.37$, c_2/c_4 equal to 22% of the point charge value, and c_6/c_4 equal to 4.5 times the point charge value. The energy scale corresponds to that used in the later calculations of resonant field.

levels for the four sites as a function of angle in (110) for a typical c_2/c_4, c_6/c_4 and λ.

The four near crossings in the (110) plane are seen to be contributed by the four sites in the following way; one site yields two near crossings, two yield one each,

and one yields none. All choices of the parameters which were considered satisfactory, assigned near crossings to the sites in the same way. Since the crystallographically-inequivalent sites differ only by a rotation, each position of the applied field in the actual (110) plane furnishes

information about the energy levels of the Hamiltonian (5) for four different values of $\mathbf{n}_i$. Motion of the applied field through 90° in the (110) plane then explores four 90° segments of great circles in the space of $\mathbf{n}$. In Fig. 13 is shown one octant in the $\mathbf{n}$ space referred to the local orthorhombic axes. The positions of the $\mathbf{n}$ which correspond to the various near crossings in the (110) plane are indicated. It will be seen that the 18°, 38°, and 78° points fall on a single curve, while the 90° peak is isolated. Assuming that the single curve is now a locus of near-crossings, one may examine the data of Fig. 2 taken in other crystallographic planes and assign the peaks and their observed angular positions to particular sites in a unique way so that all of them fall on the same single curve or belong to the isolated peak (see Fig. 13). This does not require additional computations.

Parenthetically, we note that the complexity of the observed field for resonance surface arises from the multiplicity of inequivalent sites as shown in Fig. 14.

We may conclude that if the position of the two lowest levels is considered as a function of the direction of the exchange field, we have a rather simple locus for their near crossing. The peak at 90° in (110), or the y axis of the local system (Fig. 13) is allowed by symmetry to be an isolated minimum of the level separation. Actually, the region between this point and the main line of crossings (in the local yz plane) is rather complicated since it appears that *three* levels are close together here. The interplay of the three levels makes the behavior rather sensitive to the values of the parameters in the Hamiltonian. Some additional calculations were made in the local yz plane to make sure that the final parameters used reproduced the behavior in this plane correctly [as deduced from the measurements in the crystallographic (100) plane].

Calculation of Field for Resonance

The equation of motion of the majority lattice is

$$(1/\gamma)(d/dt)(\mathbf{M}_0+\mathbf{m}) = (\mathbf{M}_0+\mathbf{m})\times(\mathbf{H}_{\text{eff}}+\mathbf{h}), \quad (6)$$

where γ is the gyromagnetic ratio, $\mathbf{M}_0$ the dc magnetization, and $\mathbf{m}$ the rf magnetization of the majority lattice. $\mathbf{H}_{\text{eff}}$ is the effective dc field acting on the majority lattice, which is the sum of the applied magnetic field $\mathbf{H}_0$ and the dc exchange field from the terbium. $\mathbf{h}$ is the rf exchange field of the terbium. We assume a spherical sample and drop all demagnetizing terms. We also ignore the anisotropy due to the iron sublattice; this may very roughly be put in at the end as an additive correction to the applied field. If a cartesian system of axes, ξ, η, ζ be chosen with ζ coinciding with the dc magnetic field direction, the small signal version of (6) becomes, for an angular frequency ω,

$$i(\omega/\gamma)m_\xi = m_\eta H_{\text{eff}} - |M_0|h_\eta,$$
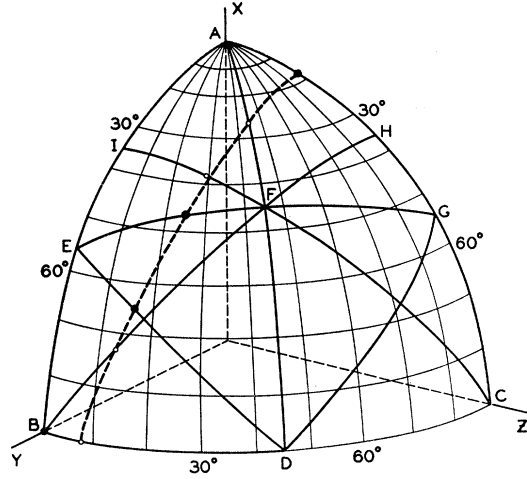$$i(\omega/\gamma)m_\eta = -m_\xi H_{\text{eff}} + |M_0|h_\xi. \quad (7)$$

FIG. 13. Locus of near crossings of the two lowest-energy levels as a function of the relative directions of the magnetization and the local orthorhombic axes of a site. x, y, and z are the site axes. When the magnetic field is turned in the (110) plane, the arcs AB, AC, DEF, and DGZ are explored; when it is turned in the (100) plane, arcs BC and AD are searched; finally, the (111) crystal plane corresponds to arcs BH and CI. The four solid circles represent the four near crossings found experimentally in the (110) plane; their assignment to sites is based upon computation. The four open circles represent near crossings found in other crystallographic planes and the assignment to sites is based upon plausibility.

H_{eff} will be given by the expression

$$H_{\text{eff}} = H_0 - \sum_i A_i\langle J_{\zeta i}^0\rangle, \quad (8)$$

where the A_i are constants which will be discussed below and $\langle J_{\zeta i}^0\rangle$ is the dc component along the ζ axis of the angular momentum vector J_i representing the terbium ions on the ith type of site. Similarly, $h_{\eta,\xi}$ will be given by $A_i\langle J_{\eta,\xi};_i^1\rangle$ where the superscript "1" refers to the rf component of $\mathbf{J}_i$ induced by the rf component,
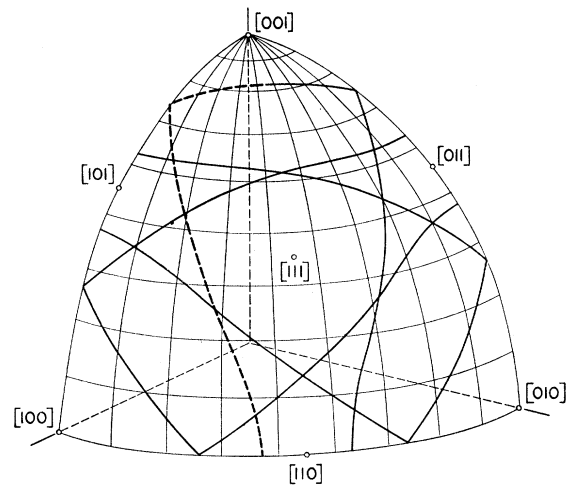

FIG. 14. The complexity of the observed H_{res} surface of YIG(Tb) at liquid helium temperatures arises from the multiplicity of inequivalent sites. This figure shows an octant of the crystal coordinate system on which are plotted the loci of close approaches of the six inequivalent sites, one of which was given in Fig. 13.

$\lambda(\mathbf{m}\cdot\mathbf{J}/|\mathbf{M}_0|)$, of the iron exchange field. The calculation of $J_{\zeta,i}{}^0$ is straightforward when the eigenfunctions of the Hamiltonian are known. Provision was made to calculate it at finite temperatures as well as in the ground state.

The calculation of $\langle\mathbf{J}^1\rangle$ may be carried out by the usual methods of first-order time-dependent perturbation theory. If we write

$$\langle J_\alpha{}^1\rangle = \sum_\beta T_{\alpha\beta}m_\beta; \quad \alpha,\beta=\xi,\eta; \qquad (9)$$

then $T_{\alpha\beta}$; which is identical with the susceptibility up to a multiplicative constant, is given by

$$T_{\alpha\beta}=\frac{-\lambda}{|M_0|}\sum_{mn}(\rho_{mm}{}^0-\rho_{nn}{}^0)$$
$$\times\left(\frac{J_{mn}{}^\alpha J_{nm}{}^\beta}{\omega+E_n-E_m}+\frac{J_{nm}{}^\alpha J_{mn}{}^\beta}{\omega-E_n+E_m}\right); \qquad (10)$$

where $\rho^0=e^{-\beta H}/\text{Trace } e^{-\beta H}$, the normalized density matrix; E_m, $m=1$ to 13, are the energy levels of the terbium; and $J_{mn}{}^\alpha$, is the matrix element of J^α between states m and n. ω must be expressed in the same dimensionless form as the other energies.[8] We note that in computing the T matrix, the matrix elements of J are evaluated first in the local axis system to which the Hamiltonian is referred and then properly rotated to give the required components along ξ and η. The computer program again provided for computing the T matrix at finite temperatures.

The above relations connect $\mathbf{h}$ and $\mathbf{m}$ and after they are substituted in (7) one finds that H_{eff} satisfies the equation

$$(H_{\text{eff}}-|M_0|\sum_i A_i T_{\eta\eta,i})(H_{\text{eff}}-|M_0|\sum_i A_i T_{\xi\xi,i})$$
$$=|(i\omega/\gamma+|M_0|\sum_i A_i T_{\xi\xi,i})|^2. \qquad (11)$$

It will be noted that Eq. (11) contains H_0 in such combinations as

$$H_0-\sum_i A_i\langle J_{\xi,i}{}^0\rangle-|M_0|\sum_i A_i T_{\eta\eta,i}.$$

If one treated a system of two sublattices, with crystal fields weak compared to the exchange fields, in a manner similar to that used here, the analog of the above expression would be

$$H_0+H_{\alpha 1}+\lambda M_2-\frac{\lambda^2 M_2 M_2}{\omega/\lambda+H_0+H_{\alpha 2}+\lambda M_1},$$

where M_1 and M_2 are the sublattice magnetizations, λ the exchange constant, and $H_{\alpha 1}$ and $H_{\alpha 2}$ effective anisotropy fields. If $\lambda M_1\gg\omega/\gamma+H_0+H_{\alpha 2}$, then the

leading term in the expansion of the fraction cancels the term λM_2 and the whole expression depends upon λ only to order $1/\lambda$. This corresponds to the familiar fact that the exchange does not appear normally in the field for resonance. When the crystal field is comparable with the exchange field there is no reason for the dc exchange field of one sublattice to be cancelled by a term from its rf susceptibility. Thus, it is possible to have a more or less angularly insensitive displacement of the field for resonance.

The constants A_i which appear in the expressions for the effective fields are related to the choice of an energy scale. We may suppose that there is an energy C_0 such that when (5) is multiplied by C_0/λ it becomes the true single-ion Hamiltonian. C_0 is clearly given by the expression

$$\kappa|M_0|\sigma_{\text{Tb}}/|J|.$$

One method of estimating C_0 is to use the value of κ found by Pauthenet[4] for TbIG. This analysis, however, ignores the crystal field effects entirely. A somewhat better method is to calculate a magnetization curve for TbIG for some set of the parameters in the Hamiltonian and various values of C_0. C_0 is then chosen to give the best fit to the observed magnetization.[9] This method again assumes that the crystal field in TbIG at the dodecahedral sites is the same as that in doped YIG
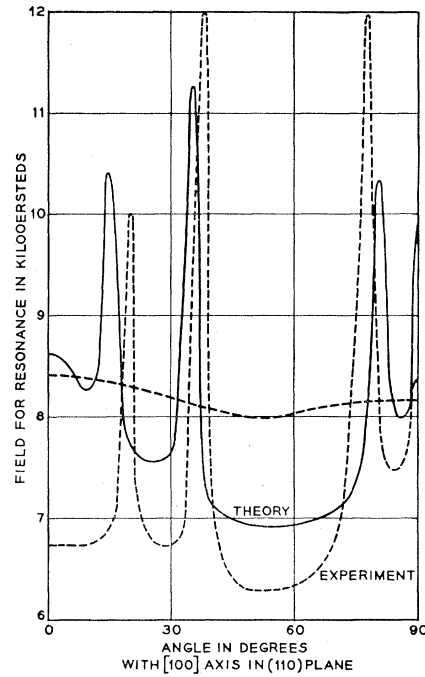

FIG. 15. Comparison between the experimental and computed fields for resonance in the (110) plane for a concentration of 0.1%, $c_2/c_4=0.22$, $c_6/c_4=4.5$, $\lambda=0.3$. The smooth broken curve shows the field for resonance without doping. The iron ion anisotropy deduced from this has been included in the computed fields.

---

[8] It is to be noted that if ω is ignored, the fractions in the sum for $T_{\alpha\beta}$ are essentially those which arise in finding the second-order perturbation of the energy levels when the field is deviated through a small angle. They are thus connected with quantities like $\partial^2 E_n/\partial\theta\partial\varphi$, where θ and φ are the polar angles of the exchange field. This establishes the connection with the *curvature* of the energy levels which occurs in Kittel's treatment.[3] Curvature, in fact, indicates both a near crossing and a significant matrix element between the close levels.

[9] The magnetization of single crystal terbium iron garnet has been measured recently by H. J. Williams and R. C. Sherwood (private communication).

and that Tb−Tb exchange is negligible. Properly, C_0 should be optimized for every different set of parameters used in the Hamiltonian, before the field for resonance is calculated.

The constants A_i are now found in the following way. The effective exchange field of the terbium is κM where M is the terbium magnetic moment. If the number of dodecahedral sites be N, the concentration of terbium, written as the fraction of dodecahedral sites occupied by terbium ions, be c, and f_i be the fraction of dodecahedral sites of the ith kind, then

$$M(\text{terbium}) = \sum_i N c f_i (\sigma_{\text{Tb},i}), \qquad (19a)$$

$$J A_i = N c f_i \kappa (\sigma_{\text{Tb},i}), \qquad (19b)$$

$$A_i = N c f_i \kappa |\sigma_{\text{Tb}}/J| = N c f_i (C_0/|M_0|). \qquad (19c)$$

DISCUSSION

While the results obtained in locating the near crossings were very satisfactory and must give a reliable picture of the relative positions of the two lowest states, it was remarked earlier that many combinations of parameters gave equally good results. It was hoped that the calculations of the field for resonance would lead to a sharper determination of the parameters, but this turned out not to be the case. In fact it becomes clear, that the model with three adjustable parameters is really not capable of reproducing the observed data with satisfactory accuracy.

In the first place, the calculated magnetization curve for TbIG may be made (by suitable choice of C_0) to fit the observed curve from about 35° upward but disagrees by about 8% at 0°K; the calculated value is the larger. This may be due to a real difference between the crystal fields of TbIG and YIG, which would be most conspicuous at very low temperatures. We have chosen to use the value of C_0 which gives the best fit at higher temperatures. This estimated value of C_0 seems to vary rather slowly with the parameters in the Hamiltonian, so that in view of other shortcomings in the calculation we have not recalculated C_0 for each case. C_0 may be considered to lie between 22° and 27°K which is substantially higher than Pauthenet's value.

Calculations of the field for resonance in the (110) plane were carried out for an extensive series of values of λ, c_2/c_4, and c_6/c_4; each set of such values was chosen to put the near crossings within two or three degrees of their correct positions. There is, unfortunately, some uncertainty about the terbium concentration in the samples for which data was taken. Most of the calculations were done for $C = 0.1\%$; a later determination of C gave a value of 0.19% and some further computation was done for this value. In either case a rather wide variety of parameters gave a fit of about the same quality. The latter may be described roughly by saying that if each peak was held to within ±2° of its correct position then at least one peak height would be in error by a factor of two.
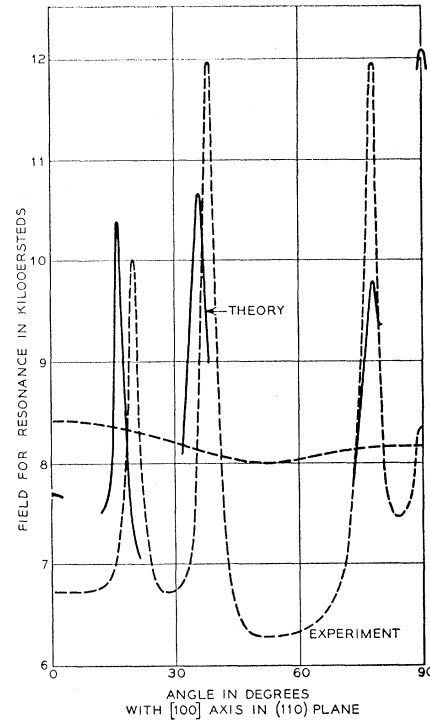

FIG. 16. Fields for resonance in the (110) plane for a concentration of 0.19% and $c_2/c_4 = 0.37$, $c_6/c_4 = 2.7$, $\lambda = 0.47$. A complete field for resonance curve was not computed; the points computed for 0° and 90° are shown by small arcs.

Figure 15 shows the best fit which was obtained with the lower value of the concentration. Its main shortcoming is the poor agreement near $\theta = 0°$, where the observed depression of the field for resonance has been lost. It should be noted that the value of c_2/c_4 used here is very small; about 22% of the nominal (point charge) value and that of c_6/c_4 correspondingly large. This might be due to a screening of the $4f$ electrons, principally for small values of r, which would decrease $\langle r^2 \rangle$ relative to $\langle r^4 \rangle$. Using the larger value for the concentration substantially larger values of c_2/c_4 give a good fit. An incomplete curve of the field for resonance is shown in Fig. 16 for $c_2/c_4 = 0.37$ and $c_6/c_4 = 2.7$. The background depression of the field is now well reproduced everywhere, and the least satisfactory feature is the exaggeration of the peak at 90°.

It was not felt that the quality of the fit obtained warranted calculations of the effect of temperature upon the field for resonance. An expression for the peak heights at low temperatures, at which only the two lowest are occupied, will contain a factor $\tanh$ (energy separation in °K/2×temperature); with energy separations at the near crossings of about 5°K, which we may deduce from our value of C_0, one expects to see the peak height fall to half value within 2 or 3 degrees of 0°K. This is qualitatively in agreement with the data.

One might expect the crossing with the closest approach to be the one to exhibit most markedly the fre-

quency effect upon peak height, since the frequency tends to bridge the gap. This is not observed in fact.

There is also an effect of frequency which arises from the associated change in the magnetic field. An increase in frequency and thus of field is equivalent to a decrease in λ with the other parameters left undisturbed. We have confirmed that the three movable levels in the (110) plane (the 90° peak does not move) shift in angle with λ in the sense implied by the data of Fig. 11.

ACKNOWLEDGMENTS

APPENDIX

The potential at a terbium site arising from the eight nearest-neighbor oxygen ions may be written

$$V = (2e^2/L_0)[\lambda_0'V_2{}^0 + \lambda_2'V_2{}^2 + \mu_0'V_4{}^0 + \mu_2'V_4{}^2$$
$$+ \mu_4'V_4{}^4 + \nu_0'V_6{}^0 + \nu_2'V_6{}^2 + \nu_4'V_6{}^4 + \nu_6'V_6{}^6],$$

where, in the point charge approximation,

$V_2{}^0 = 2z^2 - x^2 - y^2,$ $\lambda_0' = 11.75,$

$V_2{}^2 = x^2 - y^2,$ $\lambda_2' = 15.84,$

$V_4{}^0 = 8z^4 - 24z^2(x^2+y^2) + 3(x^2+y^2)^2,$ $\mu_0' = -1460.2,$

$V_4{}^2 = 4(x^2-y^2)(6z^2-x^2-y^2),$ $\mu_2' = 40.0,$

$V_4{}^4 = x^4 - 6x^2y^2 - y^4,$ $\mu' = 5118.2,$

$V_6{}^0 = 32z^6 - 240z^4(x^2+y^2)$
$\quad + 180z^2(x^2+y^2)^2 - 10(x^2+y^2)^3,$ $\nu_0' = -6300.9,$

$V_6{}^2 = 15(x^2-y^2)[16z^4 - 16z^2$
$\quad \times (x^2+y^2) + (x^2+y^2)^2],$ $\nu_2' = 28\,850.5,$

$V_6{}^4 = 6(x^4 - 6x^2y^2 + y^4)$
$\quad \times (10z^2 - x^2 - y^2),$ $\nu_4' = 909.5,$

$V_6{}^6 = x^6 - 15x^4y^2 + 15x^2y^4 - y^6,$ $\nu_6' = 4791.7.$

x, y and z are measured in units of $L_0 = 1.2376 \times 10^{-8}$ cm, the lattice constant[4] of YIG. The $V_{2n}{}^0$ are proportional to $Y_{2n}{}^0 r^{2n}$ and the $V_{2n}{}^{2m}$ are proportional to $(Y_{2n}{}^{2m} + Y_{2n}{}^{-2m})r^{2n}$; the constant of proportionality is

$$(2n)(2)[4/(4n+1)]^{\frac{1}{2}}[(2n+2m)!(2n-2m)!]^{-\frac{1}{2}}$$

in all cases.

$\mathfrak{IC}_2$, $\mathfrak{IC}_4$ and $\mathfrak{IC}_6$ the parts of the crystal Hamiltonian

are now of the form

$$\mathfrak{IC}_2 = \lambda_0'U_2{}^0 + \lambda_2'U_2{}^2,$$
$$\mathfrak{IC}_4 = \mu_0'U_4{}^0 + \mu_2'U_4{}^2 + \mu_4'U_4{}^4, \tag{7}$$
$$\mathfrak{IC}_6 = \nu_0'U_6{}^0 + \nu_2'U_6{}^2 + \nu_4'U_6{}^4 + \nu_0'U_6{}^6,$$

where for $J = 6$

$$U_2{}^0 = 2m^2 - 42, \tag{8a}$$
$$U_2{}^2 = [J_+{}^2 + \text{c.c.}],$$

$$U_4{}^0 = 35m_+{}^4 1235m^2 + 5040,$$
$$U_4{}^2 = 2J_+{}^2[7(m+1)^2 - 40] + \text{c.c.}, \tag{8b}$$
$$U_4{}^4 = [J_+{}^4 + \text{c.c.}],$$

$$U_6{}^0 = 462m^6 - 24990m^4 + 326928m^2 - 604800,$$
$$U_6{}^2 = J_+{}^2[495(m+1)^2 - 10215(m+1)$$
$$\qquad\qquad\qquad + 21600] + \text{c.c.}, \tag{8c}$$
$$U_6{}^4 = J_+{}^4[33(m+2)^2 - 108] + \text{c.c.},$$
$$U_6{}^6 = [J_+{}^6 + \text{c.c.}],$$

where $m = J_z$, $J_+ = J_x + iJ_y$, and "c.c." indicates a complex conjugate.

The *nominal* values of c_2, c_4, c_6 are now given by

$$c_2 = 2e^2L_0{}^{-3}\alpha\langle r^2\rangle,$$
$$c_4 = 2e^2L_0{}^{-5}\beta\langle r^4\rangle,$$
$$c_6 = 2e^2L_0{}^{-6}\gamma\langle r^6\rangle,$$

where $\alpha = -1/(3^2 \times 11)$, $\beta = 2/(3^3 \times 5 \times 11^2)$, $\gamma = -1/(3^4 \times 7 \times 11^2 \times 13)$ are constants appropriate[10] to the configuration $4f^8\,{}^7F_6$. Here $\langle r^2\rangle$, $\langle r^4\rangle$, and $\langle r^6\rangle$ are the averages of the indicated powers of r, the radial coordinate, over a terbium $4f$ wave function (with r now measured in cm).

Making use of the thallium ($Z=81$) $4f$ wave functions[11] these averages have been evaluated with the results

$$\langle r^2\rangle = 7.45 \times 10^{-18} \text{ cm}^2,$$
$$\langle r^4\rangle = 1.14 \times 10^{-34} \text{ cm}^4,$$
$$\langle r^6\rangle = 3.12 \times 10^{-51} \text{ cm}^6.$$

The screening constant, σ, for $4f$ electrons is given by Ridley[12] as 41. It seems probable that the value, $\sigma = 47$, given in reference 11 is a misprint. Using Ridley's value the averages for terbium are given by

$$\langle r^2\rangle = 2.07 \times 10^{-17} \text{ cm}^2,$$
$$\langle r^4\rangle = 8.78 \times 10^{-34} \text{ cm}^4,$$
$$\langle r^6\rangle = 6.69 \times 10^{-50} \text{ cm}^6.$$

[10] K. W. H. Stevens, Proc. Phys. Soc. (London) **A65**, 209 (1952).
[11] A. S. Douglas, D. R. Hartree, and W. A. Runciman, Proc. Cambridge Phil. Soc. **51**, 486 (1955).
[12] E. C. Ridley, Proc. Cambridge Phil. Soc. **51**, 693 (1955).

The corresponding values of c_2, c_4 and c_6 are then

$$c_2 = -3.68 \times 10^{-1} {}^\circ K,$$
$$c_4 = 1.24 \times 10^{-5} {}^\circ K,$$
$$c_6 = -5.63 \times 10^{-10} {}^\circ K.$$

It was pointed out earlier that the Hamiltonian used for computing the energy levels was written in the form

$$\mathcal{3C} = \lambda(\mathbf{n}_i \cdot \mathbf{J}) + (1-\lambda)c_4'[(c_2/c_4)\mathcal{3C}_2 + \mathcal{3C}_4 + (c_6/c_4)\mathcal{3C}_6].$$

c_4' was taken arbitrarily to be 1.97×10^{-7}. As pointed out in the earlier text, when values of c_2/c_4 and c_6/c_4 are mentioned they are expressed in terms of the values of c_2/c_4 and c_6/c_4 calculated above.

Paramagnetic Resonance of Chromic Ions in Double Nitrate Crystals and Frozen Solution*

J. W. Culvahouse

Department of Physics and Astronomy, University of Kansas, Lawrence, Kansas

(Received June 12, 1961; revised manuscript received August 21, 1961)

Chromic ions are shown to enter double nitrate crystals in two different interstitial sites, and the spin Hamiltonian parameters for these ions have been determined. It is also shown that cloudy double nitrate crystals contain occluded solution and the amount of solution contained in a number of crystals has been measured. The paramagnetic resonance properties of frozen samples of the solution from which the chromium-doped double nitrate crystals were grown have been investigated. The results reported in this paper are compared with the nuclear orientation results for Cr^{51} in cerium magnesium nitrate obtained by Kaplan and Shirley. The utility of frozen solutions for nuclear orientation experiments is discussed.

I. INTRODUCTION

CERIUM magnesium and cerium zinc nitrate crystals have been used extensively in nuclear orientation experiments[1] because very low temperatures may be obtained by adiabatic demagnetization of the salt, and the small value of $g_{||}$ for the cerium ion permits the application of rather large external fields without a large rise in temperature. Nuclei of several of the rare-earth trivalent ions and iron-group divalent ions can be oriented in these crystals. Recently, Kaplan and Shirley (KS)[2] have shown that cerium magnesium nitrate crystals grown from solutions containing chromic ions do contain some chromium and that Cr^{51} nuclei thus included in the crystal can be oriented. These authors suggest that their method may be extended to a wide variety of paramagnetic ions, and this possibility enhances the interest in the clarification of the nuclear orientation mechanism or mechanisms which were operative in their experiment.

KS concluded that the chromic ions were trapped in tiny pockets of solution—"brine holes"—rather than in crystal sites. In Sec. II of this paper, electron paramagnetic resonance data are described which show that chromic ions go into two different interstitial sites of the double nitrate crystals. However, proton resonance measurements described in Sec. III show that cloudy double nitrate crystals may be grown with at least as much as 10% occluded solution by volume without any large-scale occlusions. On the other hand, clear crystals do not contain an appreciable amount of solution. In Sec. IV, the electron paramagnetic resonance properties of frozen solutions of chromic ions are discussed and qualitative estimates are made of their utility in nuclear orientation experiments.

In Sec. V, the orientation experiments reported by KS are compared with the paramagnetic resonance results. In the last section, the use of interstitial sites and occluded solution for nuclear orientation is discussed as a general method for the orientation of the nuclei of paramagnetic ions.

Note added in proof. While this paper was in press, the author found that the presence of two paramagnetic complexes in chromium-doped lanthanum zinc has been reported by Pastor and Devor [J. Chem. Phys. **31**, 1145 (1959)]. The spin-Hamiltonian parameters obtained by those authors agree with those reported in the present paper. Their results for the ratio of the concentration of chromic ions relative to rare-earth ions in the crystal to the ratio in the solution is much smaller than reported in this paper. Subsequent investigation by the author has shown that the origin of this discrepancy is the fact that the concentration of chromic ions in the crystal does not increase in direct proportion to the concentration of chromic ions in the solution.

---

[1] R. P. Hudson, *Progress in Cryogenics* (Academic Press, Inc., New York, 1961), Vol. III, p. 97.

[2] Morton Kaplan and D. A. Shirley, Phys. Rev. Letters **6**, 361 (1961).